



UDC 621.45.038.7

<https://doi.org/10.17073/1997-308X-2023-1-63-74>Research article
Научная статья

The influence of Ni on the composition, structure and properties of Ti–Cr–N coatings

A. V. Chernogor, I. V. Blinkov[✉], D. S. Belov,
V. S. Sergevnin, A. P. DemirovNational University of Science and Technology “MISIS”,
4 Leninskiy Prosp., Moscow 119049, Russian Federation biv@mis.ru

Abstract. The influence of nickel on the structure and properties of Ti–Cr–N ion-plasma coatings obtained by arc-PVD method has been studied. With a nickel content of up to 11.9 at. %, the coating consists of Cr₂N, Ti_{1-x}Cr_xN, and metallic Ni. Upon further increase in Ni concentration in the coating, intermetallic compound Ni₃Ti is formed. The structure of the coatings was studied using the transmission electron microscopy. The coatings of Ti–Cr–N system are characterized by a columnar structure, in the columns of which Ti_{1-x}Cr_xN and Ti_{1-y}Cr_yN ($x > y$) sublayers, being several nanometers thick and containing variable concentration of titanium and chromium, as well as Cr₂N sublayers of about 25 nm are formed due to the complete solubility of TiN and Cr₂N and the planetary rotation of the substrates, resulting in layer-by-layer stacking of the components of the evaporated cathodes. This structure remains intact in coatings of Ti–Cr–N–Ni system with a low nickel concentration (on the order of tenths of at. %). However, upon that, the column size refinement and an increase in biaxial compressive stresses from 6.7 to 9.7 GPa are observed, which results in an increase in hardness from 30 to 42 GPa. The coatings with a high nickel content are characterized by a multilayer architecture with an equiaxed polycrystalline structure of nanograins in layers. As Ni concentration increases, the hardness of the coating decreases to 16.7 GPa, which is associated with an increase in the fraction of relatively soft nickel in the coating and a decrease in macrostresses to –0.6 GPa. Upon that, the wear intensity increases from $3 \cdot 10^{-15}$ to $5 \cdot 10^{-15}$ m³/(N·m). The studied coatings of Ti–Cr–N and Ti–Cr–N–Ni systems are resistant to adhesive and cohesive destruction. With an increase in the nickel content upon measuring scratching, the destruction of the coatings occurs exclusively due to the plastic deformation.

Keywords: ceramic coatings, ceramic and metal coatings, wear resistance, tribology, nitrides, hardness

Acknowledgements: the study was supported by the Russian Science Foundation grant No. 19-19-00555, <https://rscf.ru/project/19-19-00555/>

The authors express their gratitude to the Doctor of engineering sciences F. V. Kiryukhantsev-Korneev for his help in conducting research on the heat resistance of coatings.

For citation: Chernogor A.V., Blinkov I.V., Belov D.S., Sergevnin V.S., Demirov A.P. The influence of Ni on the composition, structure and properties of Ti–Cr–N coatings. *Powder Metallurgy and Functional Coatings*. 2023;17(1):63–74. <https://doi.org/10.17073/1997-308X-2023-1-63-74>

Влияние никеля на состав, структуру и свойства покрытий Ti–Cr–N

А. В. Черногор, И. В. Блинков[✉], Д. С. Белов,
В. С. Сергеевнин, А. П. ДемировНациональный исследовательский технологический университет «МИСИС»
Россия, 119049, г. Москва, Ленинский пр-т, 4

✉ biv@mis.ru

Аннотация. Исследовано влияние никеля на структуру и свойства ионно-плазменных покрытий Ti–Cr–N, полученных методом arc-PVD. При содержании никеля до 11,9 ат. % покрытие состоит из Cr_2N , $\text{Ti}_{1-x}\text{Cr}_x\text{N}$ и металлического Ni. При дальнейшем увеличении концентрации Ni в покрытии образуется интерметаллид Ni_3Ti . Методом просвечивающей электронной микроскопии изучена структура покрытий. Для покрытий системы Ti–Cr–N характерно столбчатое строение структуры, в столбцах которой, вследствие полной растворимости TiN и Cr_2N и планетарного вращения подложек, приводящего к послойной укладке компонентов испаряемых катодов, образуются субслои $\text{Ti}_{1-x}\text{Cr}_x\text{N}$ и $\text{Ti}_{1-y}\text{Cr}_y\text{N}$ ($x > y$) толщиной несколько нанометров с переменной концентрацией титана и хрома и субслои Cr_2N порядка 25 нм. Данная структура сохраняется и для покрытий системы Ti–Cr–N–Ni с малой концентрацией никеля (порядка десятых долей ат. %). Однако при этом наблюдаются измельчение размера столбцов и рост дуосных сжимающих напряжений с 6,7 до 9,7 ГПа, что приводит к повышению твердости от 30 до 42 ГПа. Для покрытий с высоким содержанием никеля характерна многослойная архитектура с равноосной поликристаллической структурой нанозерен в слоях. По мере увеличения концентрации Ni твердость покрытия снижается до 16,7 ГПа, что связано с возрастанием доли относительно мягкого никеля в покрытии и уменьшением величины макронапряжений до $-0,6$ ГПа. При этом интенсивность изнашивания увеличивается с $3 \cdot 10^{-15}$ до $5 \cdot 10^{-15}$ $\text{м}^3/(\text{Н} \cdot \text{м})$. Исследуемые покрытия систем Ti–Cr–N и Ti–Cr–N–Ni обладают стойкостью к адгезионному и когезионному разрушению. С ростом содержания никеля при измержительном царапании разрушение покрытий происходит исключительно вследствие пластического деформирования.

Ключевые слова: керамические покрытия, керамикометаллические покрытия, износостойкость, трибология, нитриды, твердость

Благодарности: Исследование выполнено за счет гранта Российского научного фонда № 19-19-00555, <https://rscf.ru/project/19-19-00555/>

Авторы выражают благодарности доктору технических наук Ф.В. Кириханцеву-Корнееву (НИТУ МИСИС) за помощь в проведении исследований по жаростойкости покрытий.

Для цитирования: Черногор А.В., Блинков И.В., Белов Д.С., Сергеев В.С., Демиров А.П. Влияние никеля на состав, структуру и свойства покрытий Ti–Cr–N. *Известия вузов. Порошковая металлургия и функциональные покрытия*. 2023;17(1):64–74. <https://doi.org/10.17073/1997-308X-2023-1-63-74>

Introduction

At present, the studies of strengthening and friction-adjustable coatings are focused on their development based on multiphase systems, in which the presence of various elements and phases significantly changes the properties compared to two-component coatings [1–5]. Systems based on transition metal nitrides are characterized by enhanced mechanical properties. Thus, three-component systems Ti–Cr–N, Cr–Mo–N, and Ti–Mo–N are significantly superior to two-component systems $Me\text{--}N$ in their hardness, tribological properties, and heat resistance [3; 5–9]. Ti–Cr–N–Ni based coatings, in which chromium and titanium based nitride phases provide a combination of heat resistance [10] and high hardness [5; 7], are of interest. Due to the refinement of the nitride phase and the formation of a dispersion-hardened structure with a plastic nickel frame, the introduction of metals with low affinity for nitrogen and limited solubility in them, for instance, nickel, into nitride coatings contributes to the formation of a material with high viscosity combined with hardness [11]. The improved performance properties of these coatings will be largely determined by the capability of controlling the composition and structure of the deposited material.

An analysis of the literary sources reveals the absence of studies in this field for coatings of Ti–Cr–N–Ni

systems. In this regard, the goal was set to study the influence of nickel on the processes of structure formation, phase formation and the properties of these coatings.

Research Methods

The coatings were deposited on VK6 alloy substrates by arc-PVD method using a three-cathode vacuum-arc ion-plasma unit equipped with two magnetic drop fraction separators. The planetary rotation of the substrate holders ensures the formation of a coating with a two-level structure, including the layers obtained by rotating the substrate holders around the table axis, and the sublayers several nanometers thick with a well-defined interface, which are formed due to the rotation of the substrate holders around their axis [12]. The current strength of the arc evaporating the cathodes was determined on the basis of its value ensuring stable arc burning and the absence of a considerable amount of the droplet phase in the formed plasma flow. The current strength during the evaporation of TiNi, Cr, and Ti cathodes was 120, 120 and 130 A, respectively. All coatings were deposited for 90 min at a negative bias potential $U_b = 120$ V applied to the substrate and partial pressures of nitrogen and argon of 0.8 and 0.6 Pa, respectively.

X-ray phase analysis (XPA) was conducted using “D8 Discover” unit (Bruker AXS, Germany) with

copper radiation. The survey was performed by sliding beam method at $2\theta = 3^\circ$ and a step of 0.01° . The macrostressed state of the coatings was studied by $\sin^2\psi$ method. The binding energy and composition of the coatings were investigated by X-ray photoelectron spectroscopy (XPS) using “VersaProbeII” unit (ULVAC-PHI Inc., the USA). Photoemission was excited in monochrome radiation AlK_α with a power of 25 W and a beam diameter of 100 μm . The spectral data were collected at an analyzer transmission energy of 11.75 eV and a data collection density of 0.1 eV per step. Furthermore, the concentration profiles of the coatings obtained by sequential ion (Ar) etching at a rate of 9.4 nm/min at an ion energy of 2 keV and a raster of 2×2 mm were also examined.

The elemental composition, surface morphology of the coatings prior to and after the oxidation, and the wear track after tribological researches were studied using a JSM-7600F scanning electron microscope with JED-2300F attachment for energy-dispersive spectrometry (JEOL, Japan). The heat resistance of the coatings was evaluated by the depth of oxygen penetration into the samples of coated hard alloys. The concentration profiles of the elements along the thickness of the samples after oxidative annealing were determined by the method of glow discharge optical emission spectroscopy (GDOES). The studies were performed using “Profiler 2” device (Horiba Jobin Yvon, France). The resolution for the concentration of chemical elements contained in the coating was 0.01 at. %.

The structure of the coatings was studied using the high-resolution transmission electron microscope (TEM) JEM 2100 (JEOL, Japan). Thin coating lamellae obtained by ion etching were used as samples. Mechanical properties (hardness, Young’s modulus, elastic and plastic deformation energy ratio) were measured during indentation using “CSM MicroHardner Tester” (CSM Instruments SA, Switzerland). The scratching of coated samples was measured using the Revetest scratch tester as per the “Methodology

for Measuring Adhesion and Cohesion Strength with the Revetest Scratch Tester, available from CSM (Switzerland) MVI AKP/09” (FR.1.28.2010.07503). The friction coefficient and wear were measured using “Tribometer T50” unit (Nanovea, the USA) using the *pin-on-disk* method with Al_2O_3 counterbody, a load of 5 N, a speed of 0.1 m/s, and a track radius of 6 mm. The friction track profile was determined using the WYKO NT1100 optical profilometer (Veeco, the USA).

Results and Discussion

The elemental composition of the obtained coatings is shown in the Table. The change in the composition was achieved by different arrangement of the used cathodes (TiNi, Cr and Ti) in the corresponding evaporation blocks of the unit, taking into account the fact that up to 80 % of the evaporated material vanishes in them, in the presence of magnetic separators [12].

In the paper, the resulting coatings were designated as $Ti_xCr_{1-x}N_y-zNi$, where x is the relative concentration of chromium obtained from the ratio of the concentration of chromium to the sum of the concentrations of chromium and titanium, rel. units; y is the relative nitrogen concentration obtained from the ratio of nitrogen concentration to the sum of chromium and titanium concentrations, rel. units; z is absolute nickel concentration, at. %.

No nickel-containing phases were detected by the XPA for coatings of Ti–Cr–N–Ni systems with a nickel concentration up to 11.3 at. %. Upon that, according to XPS data, the binding energy of nickel photoelectrons in these coatings is approximately 852.4 eV, which shows the presence of the Ni metal phase only [13]. This is due to the fact that nickel is characterized by a low thermodynamic affinity for nitrogen and does not form a nitride phase in contrast to other elements of the coating [14–17]. Taking into account the low solubility of nickel in nitrides as well as the absence of its diffraction lines in the diffraction patterns, it can be

The elemental and phase composition of the coatings

Элементный и фазовый состав покрытий

Coating	Elemental composition, at. %				Phase composition
	Ti	Cr	Ni	N	
$Ti_{0.43}Cr_{0.57}N_{0.89}$	22.9	30.1	—	47	$Ti_xCr_{1-x}N$
$Ti_{0.34}Cr_{0.66}N_{0.75}-0.1Ni$	19.4	37.5	0.1	43	$Ti_xCr_{1-x}N$
$Ti_{0.15}Cr_{0.85}N_{0.51}-8.7Ni$	9.2	51.1	8.7	31	Ni, $Ti_xCr_{1-x}N$, Cr_2N
$Ti_{0.26}Cr_{0.74}N_{0.83}-10.9Ni$	12.4	36.3	10.3	41	$Ti_xCr_{1-x}N$, Ni
$Ti_{0.25}Cr_{0.75}N_{0.76}-11.3Ni$	12.5	37.2	11.3	39	$Ti_xCr_{1-x}N$, Ni
$Ti_{0.72}Cr_{0.28}N_{1.84}-13.8Ni$	21.7	8.6	13.7	56	Ni, Ni_3Ti , $Ti_xCr_{1-x}N$
$Ti_{0.94}Cr_{0.06}N_{0.70}-36.8Ni$	33.4	1.9	36.7	28	Ni, Ni_3Ti , $Ti_xCr_{1-x}N$

assumed that the coating contains nickel in *X*-ray amorphous state that corresponds to the results presented in the paper [11].

XPS spectra obtained using layer-by-layer etching method exhibit the formation of a solid solution of a complex nitride for Ti–Cr–N coating (Fig. 1). The binding energies of $N1s$ and $Ti2p_{3/2}$ are within the range of values characteristic of titanium nitride (396.6 and 455.5 eV, respectively [18]). The binding energy of $Cr2p_{3/2}$ decreases from 575.5 to 574.5 eV as the concentration of Ti increases (the binding energy of $Cr2p_{3/2}$ for CrN compound is 575.8 eV, it is 576.1 eV for Cr_2N , and 574.0 eV for metallic Cr [19]). The change in the binding energy of photoelectrons of chromium depending on its concentration and the concentration of titanium in solid solution is caused by an increase in metallic bond fraction in the complex nitride (Cr, Ti)N [20]. Its formation is possible as a result of the close crystallo-

graphic parameters of titanium and chromium nitrides as well as their high mutual solubility [21; 22].

For Ti–Cr–N–Ni coatings with a concentration of no more than 11.3 at. % Ni, the binding energies of $Cr2p_{3/2}$ and $Ti2p_{3/2}$ in layers enriched with chromium (line 1 in Fig. 2) are 574.4 and 455.5 eV. Since the diffraction lines of Cr_2N and metallic Cr were not detected in the diffraction patterns of coatings of these compositions, the shift of $Cr2p_{3/2}$ spectrum towards lower energy is caused by a phenomenon similar to coatings of Ti–Cr–N system, i.e. the formation of a complex nitride. Upon that, according to the XPS spectra of nitrogen, the binding energy of $N1s$ (397.2 eV) is higher than that in nitrides of stoichiometric composition TiN and CrN (396.6 eV [19]) that exhibits the non-stoichiometric nature of Ti and Cr nitrides and is confirmed by $N/(Ti + Cr)$ ratio, lying within the range from 0.75 to 0.83.

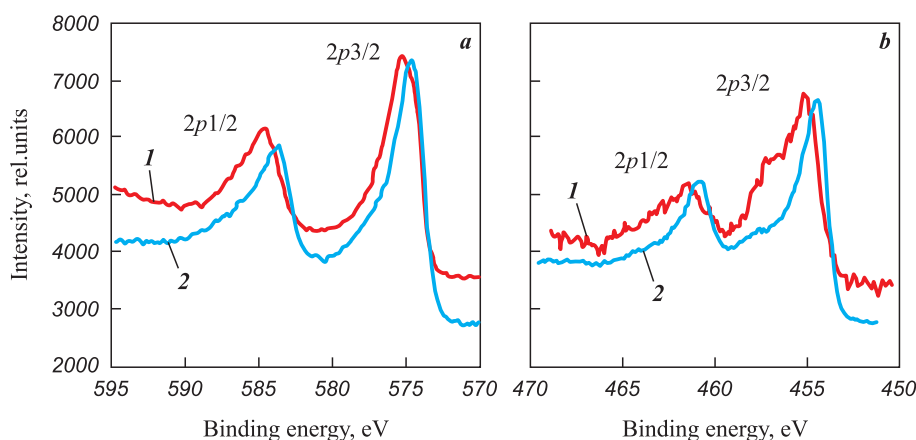


Fig. 1. XPS spectra of $Cr2p$ (a) and $Ti2p$ (b) in $Ti_{0.43}Cr_{0.57}N_{0.89}$ coating in the areas with Cr and Ti concentrations of 44 and 8 at. % (1), and 22 and 26 at. % (2), correspondingly

Рис. 1. РФЭ-спектры $Cr2p$ (a) и $Ti2p$ (b) в покрытии $Ti_{0.43}Cr_{0.57}N_{0.89}$ в областях с концентрациями Cr и Ti соответственно 44 и 8 ат. % (1) и 22 и 26 ат. % (2)

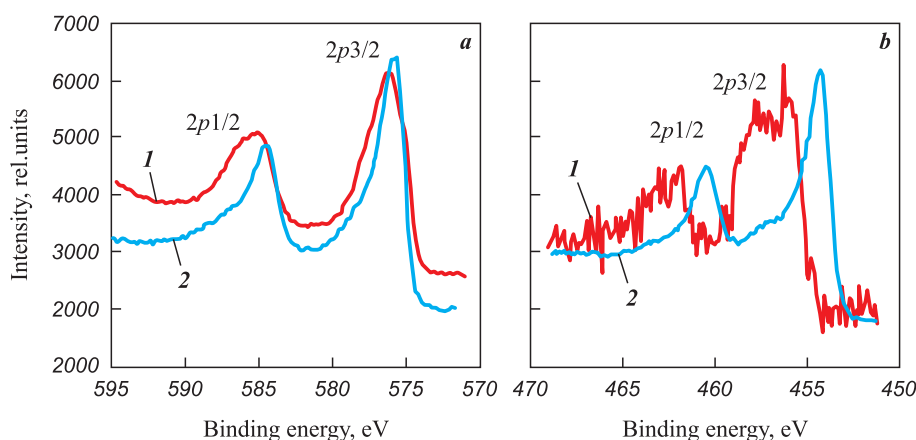


Fig. 2. XPS spectra of $Cr2p$ (a) and $Ti2p$ (b) in $Ti_{0.34}Cr_{0.66}N_{0.75-0.1}Ni$ coatings in the areas with Cr and Ti concentrations of 47 and 8 at. % (1), and 25 and 24 at. % (2), correspondingly

Рис. 2. РФЭ-спектры $Cr2p$ (a) и $Ti2p$ (b) в покрытиях $Ti_{0.34}Cr_{0.66}N_{0.75-0.1}Ni$ в областях с концентрациями Cr и Ti соответственно 47 и 8 ат. % (1) и 25 и 24 ат. % (2)

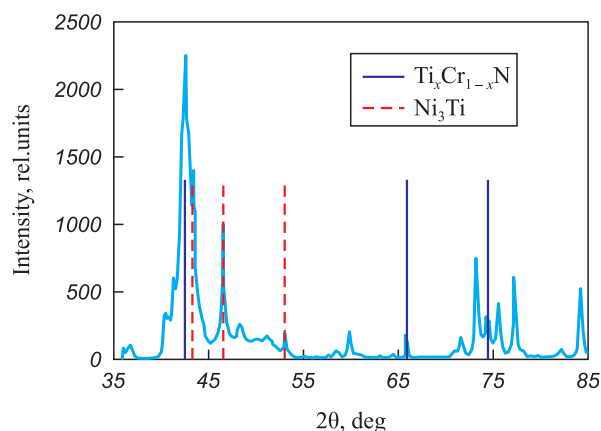


Fig. 3. The diffraction pattern of $\text{Ti}_{0.72}\text{Cr}_{0.28}\text{N}_{1.84}\text{-13.8Ni}$ coatings

Рис. 3. Дифрактограмма покрытий $\text{Ti}_{0.72}\text{Cr}_{0.28}\text{N}_{1.84}\text{-13,8Ni}$

With an increase in the nickel concentration above 13 at. % in the coating, intermetallic Ti_3Ni is formed along with $\text{Ti}_x\text{Cr}_{1-x}\text{N}$ solid solution and metallic nickel, as can be seen in the diffraction pattern for $\text{Ti}_{0.72}\text{Cr}_{0.28}\text{N}_{1.84}\text{-13.8Ni}$ coatings (Fig. 3).

The increase of the nickel concentration in Ti-Cr-N-Ni coatings is accompanied by a change in their morphology (Fig. 4). The coatings with a nickel concentration of less than 13.8 at. % are characterized by a dense cellular surface, the formation of which is caused by the replica of the substrate surface by the coating. With increasing Ni concentration, the coatings turn loose and rough due to the formation of a large amount of the droplet phase, which poorly wets the nitrides [11].

According to TEM data (Fig. 5), nickel also affects the coating structure. Thus, for Ti-Cr-N systems, the coatings exhibit a columnar structure with a column size of about 400–500 nm (Fig. 5, a). The introduction of nickel into this system at concentrations up to 3 at. % causes the refinement of the structure, which is still characterized by well-defined columns elongated in the direction of coating growth, about 220–300 nm in size (Fig. 5, b). Upon that, the TEM images for these samples clearly show that the columns consist of sublayers with a thickness ranging from several nanometers to 25 nm. According to the modeling of plasma mass trans-

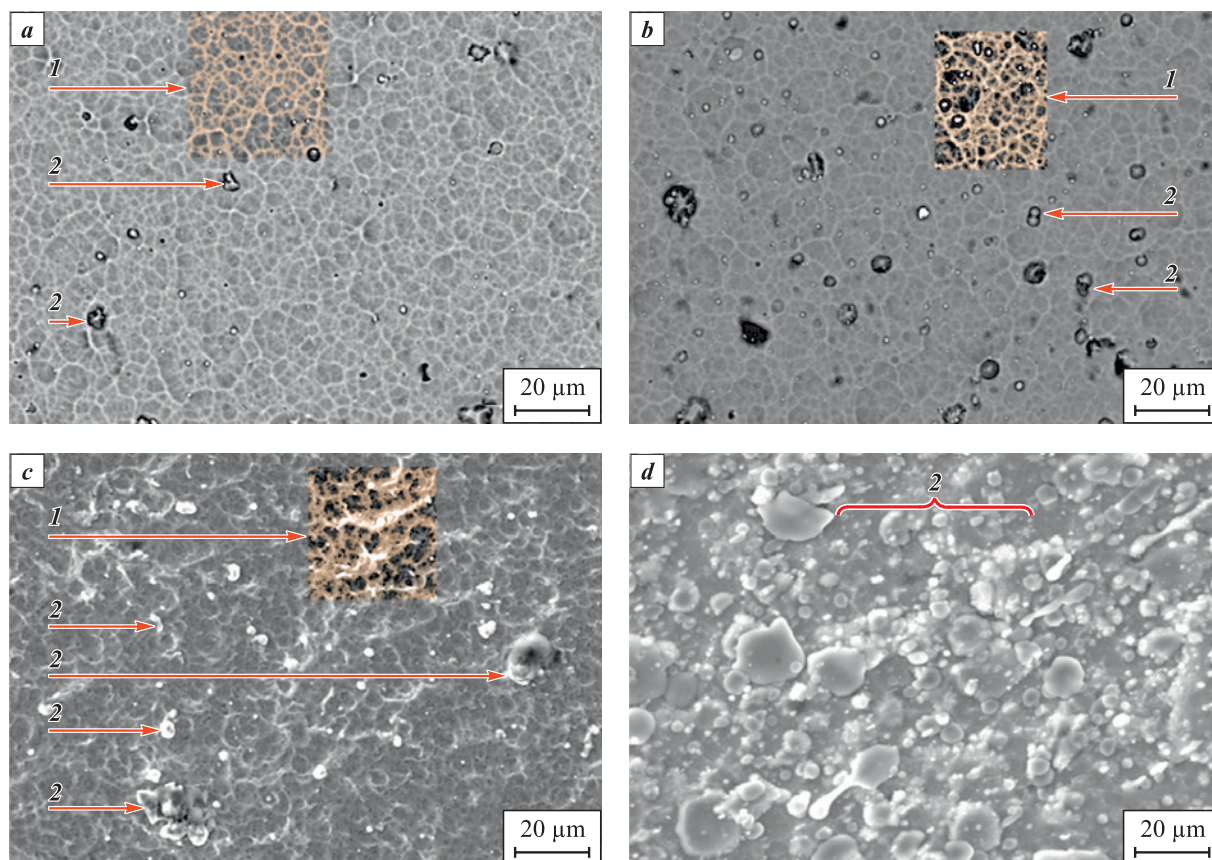


Fig. 4. The morphology of coatings of Ti-Cr-N and Ti-Cr-N-Ni systems
a – $\text{Ti}_{0.43}\text{Cr}_{0.57}\text{N}_{0.89}$, b – $\text{Ti}_{0.34}\text{Cr}_{0.66}\text{N}_{0.75}\text{-0.1Ni}$, c – $\text{Ti}_{0.15}\text{Cr}_{0.85}\text{N}_{0.51}\text{-8.7Ni}$, d – $\text{Ti}_{0.94}\text{Cr}_{0.06}\text{N}_{0.70}\text{-36.8Ni}$
1 – the elements of the cellular structure of the surface, 2 – droplet phase

Рис. 4. Морфология покрытий систем Ti-Cr-N и Ti-Cr-N-Ni
a – $\text{Ti}_{0.43}\text{Cr}_{0.57}\text{N}_{0.89}$, b – $\text{Ti}_{0.34}\text{Cr}_{0.66}\text{N}_{0.75}\text{-0,1Ni}$, c – $\text{Ti}_{0.15}\text{Cr}_{0.85}\text{N}_{0.51}\text{-8,7Ni}$, d – $\text{Ti}_{0.94}\text{Cr}_{0.06}\text{N}_{0.70}\text{-36,8Ni}$
1 – элементы ячеистой структуры поверхности, 2 – каплевая фаза

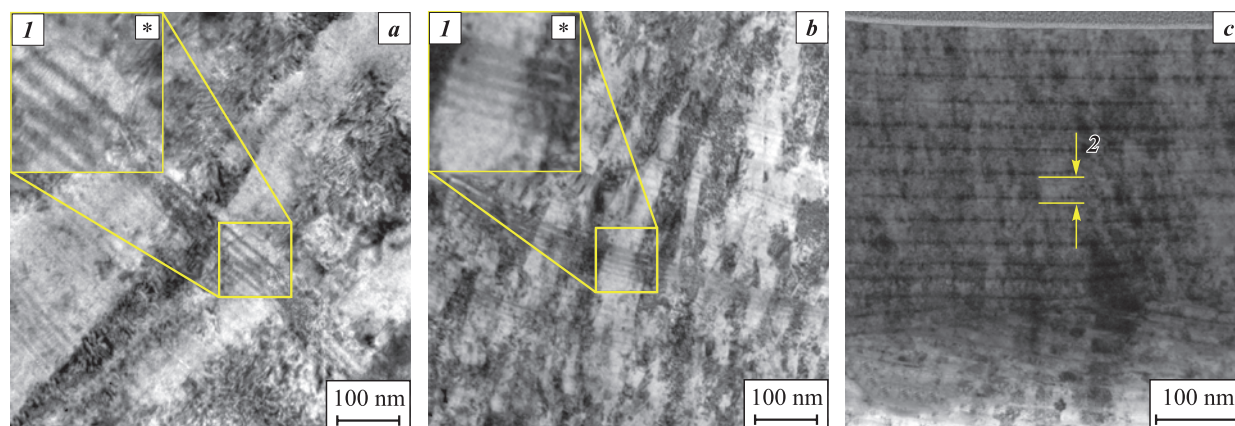


Fig. 5. The TEM image of the cross section of Ti–Cr–N–Ni coatings formed at $U_b = 120$ V

a – $\text{Ti}_{0.43}\text{Cr}_{0.57}\text{N}$, *b* – $\text{Ti}_{0.34}\text{Cr}_{0.66}\text{N}-0.1\text{Ni}$, *c* – $\text{Ti}_{0.26}\text{Cr}_{0.74}\text{N}-10.9\text{Ni}$
1 – sublayers in column volume, *2* – modulation period

Рис. 5. ПЭМ-изображение поперечного сечения покрытий Ti–Cr–N–Ni, сформированных при $U_b = 120$ В

a – $\text{Ti}_{0.43}\text{Cr}_{0.57}\text{N}$, *b* – $\text{Ti}_{0.34}\text{Cr}_{0.66}\text{N}-0.1\text{Ni}$, *c* – $\text{Ti}_{0.26}\text{Cr}_{0.74}\text{N}-10.9\text{Ni}$
1 – субслои в объеме столбцов, *2* – период модуляции

fer and the growth of coatings of these systems [23], they are caused by planetary rotation of substrates relative to evaporating cathodes and consist of solid solutions of variable concentrations of titanium and chromium ($\text{Ti}_{1-x}\text{Cr}_x\text{N}$ and $\text{Ti}_{1-y}\text{Cr}_y\text{N}$ ($x > y$)) and Cr_2N . With a subsequent increase in the nickel concentration up to 12 at.%, the coatings are already characterized by a multilayer polycrystalline architecture with a modulation period of 25 nm and an average grain size of 18 nm (Fig. 5, c). These results may show that, due to the low solubility of nickel in nitrides, it prevents their growth, refines the structure, and changes the architecture of the coatings.

$\text{Ti}_{0.43}\text{Cr}_{0.57}\text{N}_{0.89}$ and $\text{Ti}_{0.34}\text{Cr}_{0.66}\text{N}_{0.75}-0.1\text{Ni}$ coatings are characterized by high compressive macrostresses, being 6.7 and 9.7 GPa, respectively. It is known that compressive macrostresses for nitride coatings obtained by the method of ion-plasma vacuum-arc deposition can range from 4 to 12 GPa. The formation of such a “highly stressed” structure is associated, first of all, with its defectiveness: during the deposition of coatings, the flow of high-energy particles bombarding the surface contributes to the appearance of a large number of point and linear defects [24]. The introduction of nickel increases the magnitude of macrostresses due to the refinement of nitride grains, bearing in mind that an increase in the interface length leads to an increase in the number of grain boundary defects. For coatings with a high nickel content (>12 at. %), there is a significant decrease in macrostresses due to the effect of their relaxation caused by plastic deformation of nickel in the field of emerging stresses.

The thermal stability of the composition and structure of the coatings was studied after their high-temperature annealing in vacuum at temperatures of 650

and 850 °C. For Ti–Cr–N and Ti–Cr–N–Ni samples with a low nickel content, it is typical (Fig. 6) that the diffraction lines corresponding to TiCrN compound split into TiN and CrN during the annealing. This is most likely due to the dissolution of the adjacent sublayers $\text{Ti}_{1-x}\text{Cr}_x\text{N}$ and $\text{Ti}_{1-y}\text{Cr}_y\text{N}$ ($x > y$) with different concentrations of titanium and chromium, thus forming solid solutions of average composition enriched with titanium and chromium, which we observe in the diffraction patterns. These conclusions are also confirmed by the TEM images (Fig. 7), demonstrating an increase in the average grain size after the annealing.

According to the XPS data, during oxidative annealing of $\text{Ti}_{0.43}\text{Cr}_{0.57}\text{N}_{0.89}$ coatings with a chromium concentration of 27 at. % at $t = 800$ °C, Cr_2O_3 and TiO_2 phases are formed, the oxygen concentration in the coating is $\sim 4\div 5$ at. % with an oxidized layer thickness of about 0.25 μm (Fig. 8). Upon that, the coating remains intact. With an increase in the oxidation temperature to 850 °C, the oxygen content in the coating of this composition increases to ~ 19 at. %. Taking into account considerable differences in the molar volumes of titanium oxide and nitride, the surface layer of the coating becomes loose, its barrier functions with respect to oxygen decrease, the depth of oxygen penetration into the coating reaches 0.8 μm , as evidenced by the data of GDOES (Fig. 9). The analysis of the surface of the coatings by SEM method (Fig. 9) in this case demonstrated the destructive oxidation of samples of this composition, which is characterized by a local breaking of the coating to the substrate.

As the chromium concentration increases to 36 at. %, the fraction of oxygen in the coating after oxidative annealing at $t = 850$ °C decreases to 14 at. % with a decrease in the depth of the oxidized layer to 0.4 μm , but

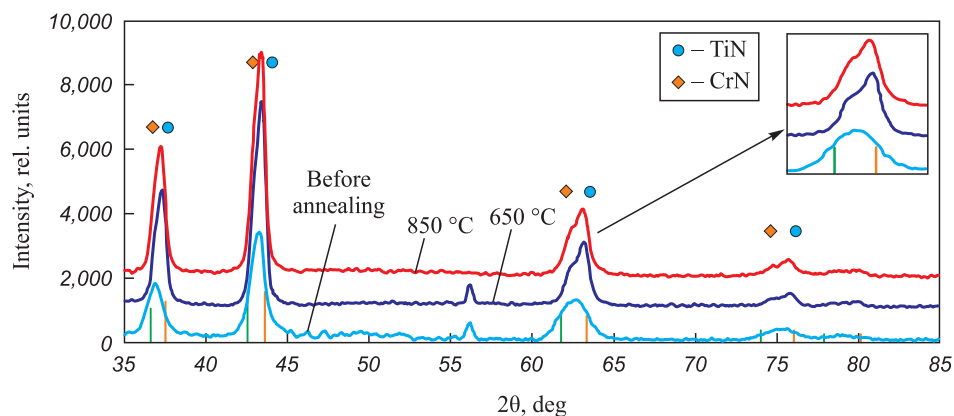


Fig. 6. The diffraction patterns of Ti–Cr–N coatings prior to and after the annealing

Рис. 6. Дифрактограммы покрытий Ti–Cr–N до и после отжига

the areas of local breaking of the coating to the substrate are still observed on the surface of the samples (Fig. 10).

The microindentation method was used to obtain data on the hardness of the studied coatings (Fig. 11), according to which $\text{Ti}_{0.34}\text{Cr}_{0.66}\text{N}_{0.75}\text{--}0.1\text{Ni}$ coatings are characterized by the highest hardness (about 42 GPa),

which can be explained by a high level of compressive macrostresses [25], being 9.7 GPa. With an increase in the nickel concentration, the hardness of the coatings decreases to 16 GPa (with a nickel content of 13.8 at. %), which is associated with an increased concentration of plastic metal phase Ni in the coating composition.

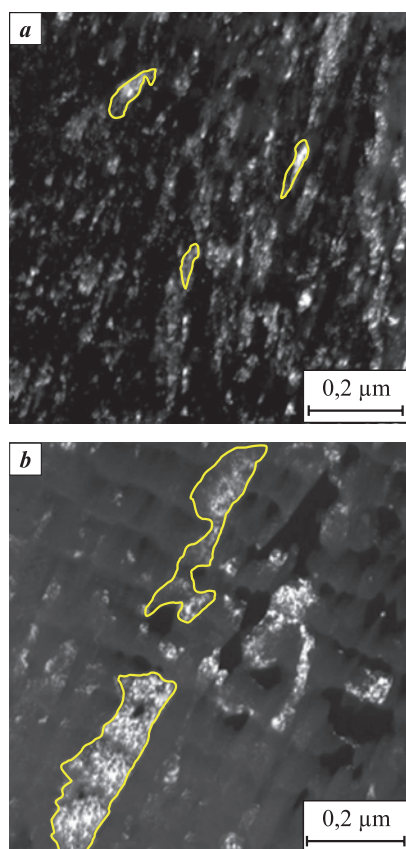


Fig. 7. The TEM images of the structure of Ti–Cr–N–Ni samples prior to (a) and after (b) the annealing

The coating grains elongated in the direction of growth are identified

Рис. 7. ПЭМ-изображения структуры образцов Ti–Cr–N–Ni до (a) и после (b) отжига

Выделены вытянутые в направлении роста зерна покрытий

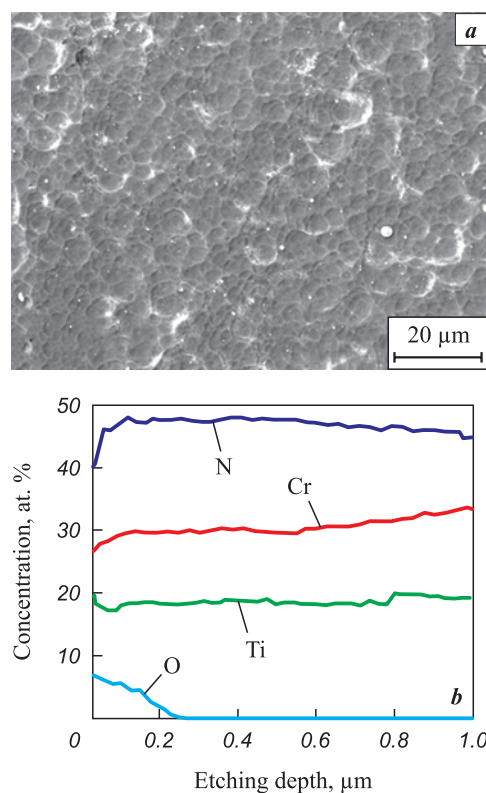


Fig. 8. The image of the surface (a) and the concentration profile of the distribution of elements (b) in $\text{Ti}_{0.43}\text{Cr}_{0.57}\text{N}_{0.89}\text{--}0.1\text{Ni}$ coating after oxidative annealing at $t = 800\text{ }^{\circ}\text{C}$

Рис. 8. Изображение поверхности (a) и концентрационный профиль распределения элементов (b) в покрытии $\text{Ti}_{0.43}\text{Cr}_{0.57}\text{N}_{0.89}\text{--}0.1\text{Ni}$ после окислительного отжига при $t = 800\text{ }^{\circ}\text{C}$

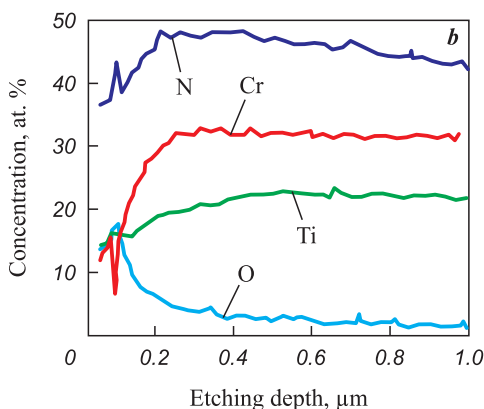
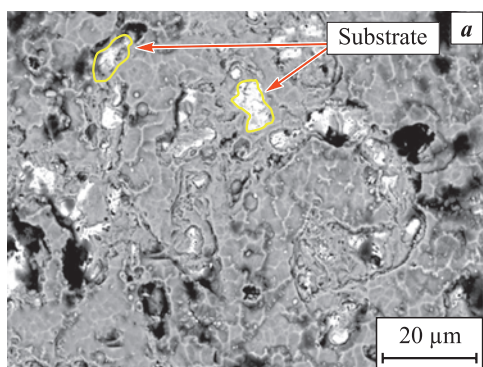


Fig. 9. The image of the surface (*a*) and the concentration profile of the distribution of elements (*b*) in $\text{Ti}_{0.43}\text{Cr}_{0.57}\text{N}_{0.89}-0.1\text{Ni}$ coating after oxidative annealing at $t = 850^\circ\text{C}$

Рис. 9. Изображение поверхности (*a*) и концентрационный профиль распределения элементов (*b*) в покрытии $\text{Ti}_{0.43}\text{Cr}_{0.57}\text{N}_{0.89}-0.1\text{Ni}$ после окислительного отжига при $t = 850^\circ\text{C}$

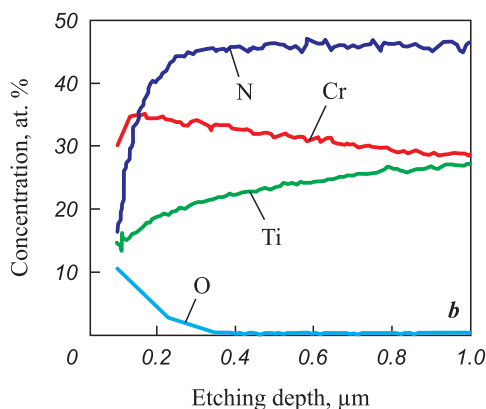
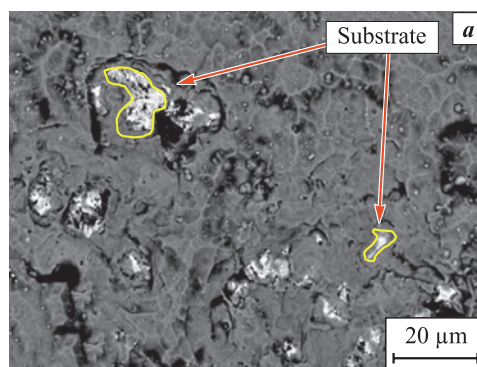


Fig. 10. The image of the surface (*a*) and the concentration profile of the distribution of elements (*b*) in $\text{Ti}_{0.34}\text{Cr}_{0.66}\text{N}_{0.75}-0.1\text{Ni}$ coating after oxidative annealing at $t = 850^\circ\text{C}$

Рис. 10. Изображение поверхности (*a*) и концентрационный профиль распределения элементов (*b*) в покрытии $\text{Ti}_{0.34}\text{Cr}_{0.66}\text{N}_{0.75}-0.1\text{Ni}$ после окислительного отжига при $t = 850^\circ\text{C}$

The results of scratch measurements (Figs. 12 and 13) indicate that up to a load of 75 N, the coatings of Ti–Cr–N and Ti–Cr–N–Ni systems (1 at. % Ni) do not exhibit any chips and cracks in the scratch body, the wear of the coating lies in partial abrasion of the protruding irregularities of the coating and plastic pressing of material out of the scratch body. When a load of 75 N is reached, cracks begin to form at the bottom of the scratch (Lc1), which is accompanied by a drastic increase in the amplitude of acoustic emission, and at a load of $\sim 85\div 87$ N (Lc3), a local appearance of the substrate occurs. Such a high fracture toughness and wear resistance during measuring scratching testify to the high cohesive strength of the coatings and their adhesion to the substrate, as determined by the high values of compressive stresses realized in the coatings [26].

An increase in the plasticity of Ti–Cr–N–Ni coating material upon the growth of Ni concentration results in a considerable change in the nature of its destruction during scratching. The coating is destroyed through plastic deformation in the entire range of applied

loads in the absence of cracking. This is evidenced by the acoustic emission data and visual observations of the scratch (Fig. 14). The destruction of the coa-

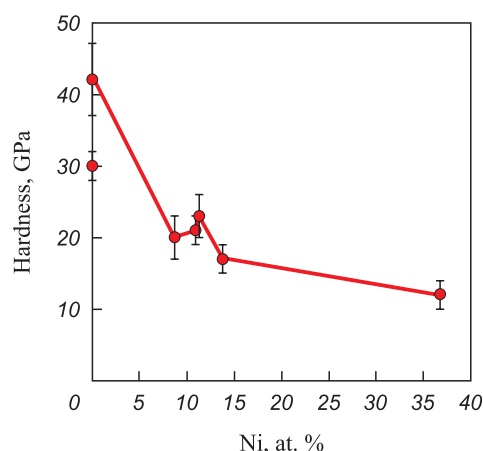


Fig. 11. The influence of nickel concentration on the hardness of Ti–Cr–N–Ni coatings

Рис. 11. Влияние концентрации никеля на твердость покрытий Ti–Cr–N–Ni

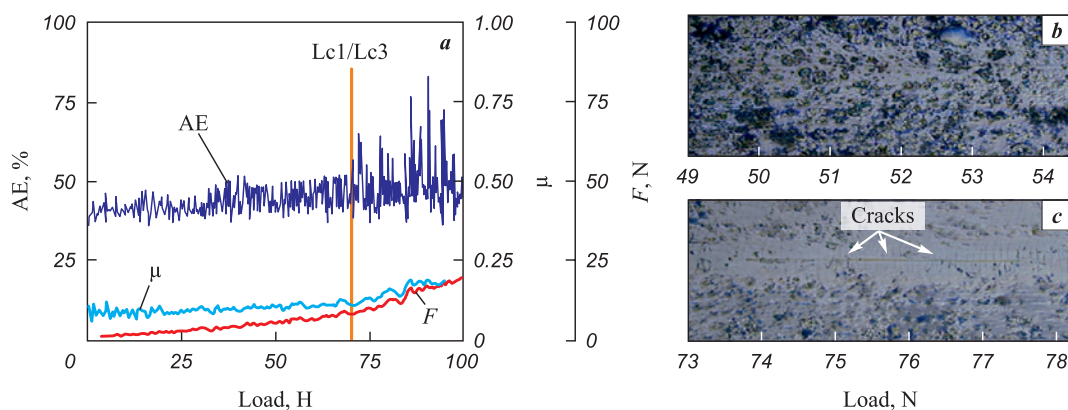


Fig. 12. The dependence of acoustic emission (AE), friction force (F) and friction coefficient (μ) on the load upon measuring scratching (**a**) and scratch images (**b, c**) for $\text{Ti}_{0.43}\text{Cr}_{0.57}\text{N}_{0.89}$ coatings

Рис. 12. Зависимость акустической эмиссии (АЭ), силы трения (F) и коэффициента трения (μ) от нагрузки при измерительном царапании (**a**) и изображения царапины (**b, c**) для покрытий $\text{Ti}_{0.43}\text{Cr}_{0.57}\text{N}_{0.89}$

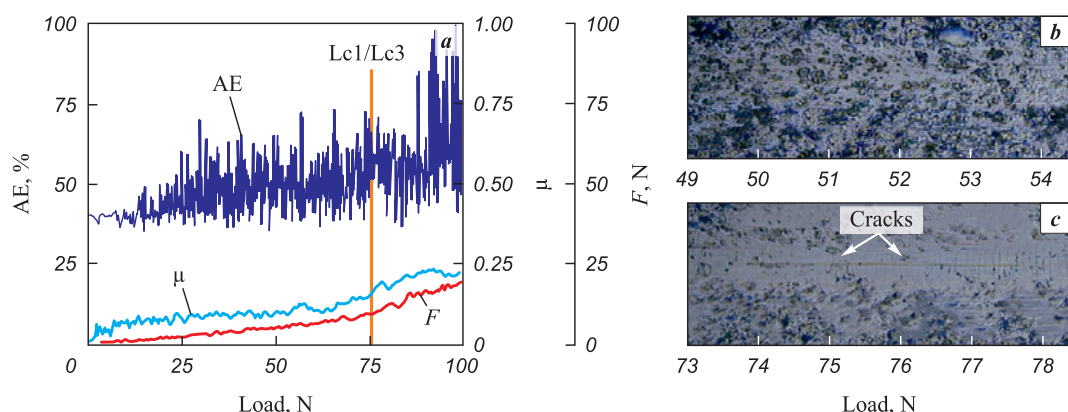


Fig. 13. The dependence of acoustic emission (AE), friction force (F) and friction coefficient (μ) on the load upon measuring scratching (**a**) and scratch images (**b, c**) for $\text{Ti}_{0.34}\text{Cr}_{0.66}\text{N}_{0.75-0.1}\text{Ni}$ coatings

Рис. 13. Зависимость акустической эмиссии (АЭ), силы трения (F) и коэффициента трения (μ) от нагрузки при измерительном царапании (**a**) и изображения царапины (**b, c**) для покрытий $\text{Ti}_{0.34}\text{Cr}_{0.66}\text{N}_{0.75-0.1}\text{Ni}$

ting occurs through the pressing of the material out of the scratch body. At loads on the indenter of more than 90 N, the coating remains intact. This type of destruction is attributed to the influence of the plastic component in its composition (Ni) on the relaxation of stresses arising in the coating during scratching.

Upon the introduction of 0.1 at. % of nickel into Ti–Cr–N coatings, the friction coefficient increases from 0.6 to 0.7 (Fig. 15). A decrease in the wear resistance of coatings is not observed, and the wear intensity is approximately $2.5 \cdot 10^{-15} \text{ m}^3/(\text{N} \cdot \text{m})$. The growth of the friction coefficient is associated with an increase in the hardness of coatings (from 30 to 42 GPa) and a decrease in their fracture toughness, as evidenced by a decrease in plastic deformation ratio (from 67 to 40 %), determined by indentation of the coating material.

As the nickel concentration in the coatings increases from 8.7 to 11.8 at. %, the wear coefficient increases

from $3 \cdot 10^{-15}$ to $4.8 \cdot 10^{-15} \text{ m}^3/(\text{N} \cdot \text{m})$, respectively. This is attributed to the relatively low hardness of the coatings.

Conclusion

Ti–Cr–Ni–N coatings obtained by arc-PVD method are composed of Cr_2N , $\text{Ti}_{1-x}\text{Cr}_x\text{N}_y$ nitrides and metallic Ni. The formation of nickel based intermetallic compounds is observed only at its concentration in the coating above 11 at. %.

The planetary rotation of the coated samples and the mutual solubility of chromium and titanium nitrides result in the formation of a complex architecture of coatings with the nickel content of tenths of at. %, consisting of columnar grains $\text{Ti}_{1-x}\text{Cr}_x\text{N}_y$, including sublayers, being several nanometers thick, which are made of Ti–Cr–N solid solution of variable composition and the sublayers of Cr_2N , being about 25 nm thick. As the nickel content in the structure of

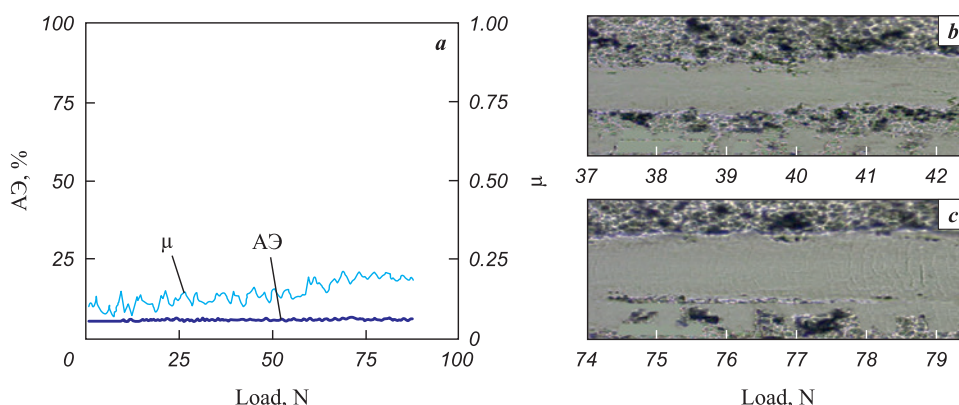


Fig. 14. The dependence of acoustic emission (AE) and friction coefficient (μ) on the load upon measuring scratching (a) and scratch images (b, c) for $\text{Ti}_{0.25}\text{Cr}_{0.75}\text{N}_{0.76}$ –11.3Ni coatings

Рис. 14. Зависимость акустической эмиссии (АЭ) и коэффициента трения (μ) от нагрузки при измерительном царапании (a) и изображения царапины (b, c) для покрытий $\text{Ti}_{0.25}\text{Cr}_{0.75}\text{N}_{0.76}$ –11,3Ni

Ti–Cr–Ni–N coatings increases, a multilayer architecture is formed.

The introduction of nickel into Ti–Cr–N coatings, resulting in the refinement of the grain structure of the nitride phase, is accompanied by an increase in compressive macrostresses from 6.7 to 9.7 GPa (at a nickel content of the order of tenths of at. %). With a further increase in its concentration, the values of compressive macrostresses decrease to 0.6 GPa, which may be caused by their relaxation through the process of plastic deformation of metallic nickel in the stress fields.

It has been established that coatings based on Ti–Cr–Ni–N multicomponent system exhibit the following properties, depending on the nickel content: hardness of 42–16 GPa; fracture toughness, characterized by the relative energy of plastic deformation, of 50–65 %; wear intensity being up to $10^{-15} \text{ m}^3/(\text{m} \cdot \text{N})$; adhesive strength with substrate (Lc3) being over 75–80 N, heat resistance being up to 850 °C. The coatings of this composition have shown high efficiency for wear protection in sea water

of a steel (20X13) liner paired with carbon fiber in sliding-surface bearings used in the friction units of ship mechanisms [27].

References / Список литературы

1. Martin P. Handbook of deposition technologies for films and coatings: Science, applications and technology. 3rd ed. Amsterdam: William Andrew, 2009. 936 p.
2. Kanoun M.B., Goumri-Said, Jacuen M. Structure and mechanical stability of molybdenum nitrides: A first-principles study. *Physical Review B*. 2007;76(13):1–4. <https://doi.org/10.1103/PhysRevB.76.134109>
3. Kazmanli M.K., Urgen M., Çakir A.F. Effect of nitrogen pressure, bias voltage and substrate temperature on the phase structure of Mo–N coatings produced by cathodic arc PVD. *Surface and Coatings Technology*. 2003;167(1): 77–82. [https://doi.org/10.1016/S0257-8972\(02\)00866-6](https://doi.org/10.1016/S0257-8972(02)00866-6)
4. Gilewicz A., Warcholinski B., Murzynski D. The properties of molybdenum nitride coatings obtained by cathodic arc evaporation. *Surface and Coatings Technology*. 2013;236:149–158. <https://doi.org/10.1016/j.surfcoat.2013.09.005>
5. Kumar D.D., Kumar N., Kalaiselvam S. Micro-tribo-mechanical properties of nanocrystalline TiN thin films for small scale device applications. *Tribology International*. 2015; 88:25–30. <https://doi.org/10.1016/j.triboint.2015.02.031>
6. Vaz F., Ferreira J., Ribeiro E. Influence of nitrogen content on the structural, mechanical and electrical properties of TiN thin films. *Surface and Coatings Technology*. 2005;191:317–323.
7. Akbarzadeh M., Shafyei A., Salimijazi H.R. Characterization of TiN, CrN and (Ti, Cr)N coatings deposited by cathodic ARC evaporation. *International Journal of Engineering*. 2014;27(7):1127–1132.
8. Shan L., Wang Y., Li J.-L., Li H., Lu X., Chen J. Structure and mechanical properties of thick Cr/Cr₂N/CrN multilayer coating deposited by multi-arc ion plating. *Transactions of Nonferrous Metals Society of China*. 2015;25(4):1135–1143. [https://doi.org/10.1016/S1003-6326\(15\)63708-6](https://doi.org/10.1016/S1003-6326(15)63708-6)

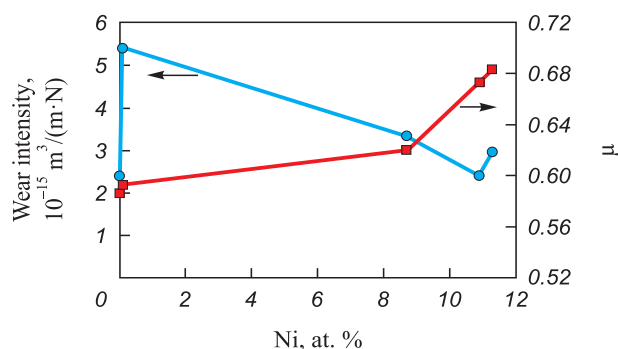


Fig. 15. The influence of nickel concentration on the tribological properties of the Ti–Cr–Ni–N coatings

Рис. 15. Влияние концентрации никеля на трибологические свойства покрытий Ti–Cr–Ni–N

9. Song G.-H., Luo Z., Li F., Chen L., He C. Microstructure and indentation toughness of Cr/CrN multilayer coatings by arc ion plating. *Transactions of Nonferrous Metals Society of China*. 2015;25(3):811–816.
[https://doi.org/10.1016/S1003-6326\(15\)63667-6](https://doi.org/10.1016/S1003-6326(15)63667-6)
10. Mayerhofer P.H., Willmann H., Mitterer C. Oxidation kinetics of sputtered Cr–N coatings. *Surface and Coatings Technology*. 2001;146–147:222–228.
[https://doi.org/10.1016/S0257-8972\(01\)01471-2](https://doi.org/10.1016/S0257-8972(01)01471-2)
11. Belov D.S., Blinkov I.V., Volkhonskii A.O. The effect of Cu and Ni on the nanostructure and properties of arc-PVD coatings based on titanium nitride. *Surface and Coatings Technology*. 2014;260:186–197.
<https://doi.org/10.1016/j.surfcoat.2014.09.069>
12. Chernogor A.V., Blinkov I.V., Belov D.S., Volkhonskii A.O. Analysis of the structure of multilayer nanocrystalline coatings based on plasma mass transfer parameters calculated by the Monte Carlo method. *Technical Physics Letters*. 2019;45(2):75–78.
<https://doi.org/10.1134/S1063785019020056>
13. Mauchamp N.A., Isobe M., Hamaguchi S. Evaluation of nickel self-sputtering yields by molecular-dynamics simulation. *Journal of Vacuum Science & Technology A*. 2021; 39(4):043005. <https://doi.org/10.1116/6.0000979>
14. Ferro R., Marazza R. The Mo–N (molybdenum–nitrogen) system. *Bulletin of Alloy Phase Diagrams*. 1980;1(2): 82–85. <https://doi.org/10.1007/BF02881198>
15. Okamoto H. N–Ti (nitrogen – titanium). *Journal of Phase Equilibria and Diffusion*. 2013;34(2):151–152.
<https://doi.org/10.1007/s11669-012-0153-6>
16. Frisk K. A thermodynamic evaluation of the Cr–N, Fe–N, Mo–N and Cr–Mo–N systems. *Calphad*. 1991;15(1): 79–106. [https://doi.org/10.1016/0364-5916\(91\)90028-I](https://doi.org/10.1016/0364-5916(91)90028-I)
17. Guillermet A.F., Frisk K. Thermodynamic properties of ni nitrides and phase stability in the Ni–N system. *International Journal of Thermophysics*. 1991;12(2):417–431.
<https://doi.org/10.1007/BF00500762>
18. Wagner C.D., Naumkin A.V., Kraut-Vass A., Allison J.W., Powell C.J., Rumble J.R.Jr. *NIST standard reference database 20*. 2003;3:251–252.
19. Lippitz A., Hübert Th. XPS investigations of chromium nitride thin films. *Surface and Coatings Technology*. 2005 200(1–4):250–253.
<https://doi.org/10.1016/j.surfcoat.2005.02.091>
20. Kunchenko Yu.V., Kunchenko V.V., Neklyudov I.M. Multilayer Ti–Cr–N coatings produced by the vacuum-arc deposition. *Voprosy atomnoi nauki i tekhniki*. 2007;(2):203–214. (In Russ.).
Кунченко Ю.В., Кунченко В.В., Неклюдов И.М. Слоистые Ti–Cr–N покрытия, получаемые методом вакуумно-дугового осаждения. *Вопросы атомной науки и техники*. 2007;(2):203–214.
21. Huang Z., Yu H., Song C., Li S. Precipitation and mechanical property of V-alloyed steel: Role of cooling rate. *Steel Research International*. 2020;91(2):1900444.
<https://doi.org/10.1002/srin.201900444>
22. Qiu, Y., Gao L. Preparation and characterization of CrN/CN and nano-TiN/CN composites. *Journal of the American Ceramic Society*. 2005;88(2):494–496.
<https://doi.org/10.1111/j.1551-2916.2005.00087.x>
23. Chernogor A.V., Blinkov I.V., Belov D.S., Sergevnin V.S., Volkhonskii A.O. Analysis of the structure of multilayer nanocrystalline coatings based on plasma mass transfer parameters calculated by the Monte Carlo method. *Technical Physics Letters*. 2019;45(2):75–78.
<https://doi.org/10.1134/S1063785019020056>
Черногор А.В., Блинков И.В., Белов Д.С., Сергеевнин В.С., Волхонский А.О. Анализ структуры многослойных нанокристаллических покрытий на основе параметров массопереноса плазмы, вычисленных методом Монте-Карло. *Письма в журнал технической физики*. 2019;45(3):16–19.
<https://doi.org/10.21883/PJTF.2019.03.47265.17575>
24. Petrov I., Hultman L., Barna P. Microstructural evolution during film growth. *Journal of Vacuum Science & Technology A*. 2003;21(5):S117–S128.
<https://doi.org/10.1116/1.1601610>
25. Veprek S., Veprek-Heijman G.J., Karvankova P. Different approaches to superhard coatings and nanocomposites. *Thin Solid Films*. 2005;476(1):1–29.
<https://doi.org/10.1016/j.tsf.2004.10.053>
26. Petrov Y., Borodin E., Cadoni E., Selyutina N.. Relaxation model for dynamic plastic deformation of materials. *EPJ Web of Conferences*. 2015;94:4039.
<https://doi.org/10.1051/epjconf/20159404039>
27. Sergevnin V.S., Anisimov A.V., Chernogor A.V., Volkhonskii A.O., Demirov A.P., Lishevich I.V., Sobolev M.Yu., Kayamutdinov Sh.D. Electrochemical stability of nitride coatings for a steel-carbon fiber tribopair under conditions of imitation of a marine environment. *Journal of Physics Conference Series*. 2021;1954(1):012040.
<https://doi.org/10.1088/1742-6596/1954/1/012040>

Information about the Authors


Alexey V. Chernogor – Junior Researcher of the Department of functional nanosystems and high-temperature materials of the National University of Science and Technology “MISIS” (NUST MISIS)

 **ORCID:** 0000-0001-5385-5369

 **E-mail:** avchernogor@gmail.com

Igor V. Blinkov – Dr Sci. (Eng.), Professor of the Department of functional nanosystems and high-temperature materials, NUST MISIS

 **ORCID:** 0000-0001-8619-6259

 **E-mail:** biv@isis.ru

Сведения об авторах


Алексей Витальевич Черногор – мл. науч. сотрудник кафедры функциональных наносистем и высокотемпературных материалов Национального исследовательского технологического университета «МИСИС» (НТУ МИСИС)

 **ORCID:** 0000-0001-5385-5369

 **E-mail:** avchernogor@gmail.com

Игорь Викторович Блинков – д.т.н, профессор кафедры функциональных наносистем и высокотемпературных материалов, НТУ МИСИС

 **ORCID:** 0000-0001-8619-6259

 **E-mail:** biv@isis.ru

Dmitry S. Belov – Cand. Sci. (Eng.), Senior Researcher of the Department of functional nanosystems and high-temperature materials, NUST MISIS

 **ORCID:** 0000-0002-7053-5540

 **E-mail:** dm.blv@yandex.ru

Viktor S. Sergevnin – Cand. Sci. (Eng.), Engineer of the Department of functional nanosystems and high-temperature materials, NUST MISIS

 **ORCID:** 0000-0002-7053-5540

 **E-mail:** v.s.sergevnin@gmail.com

Aleksandr P. Demirov – Assistant of the Department of functional nanosystems and high-temperature materials, NUST MISIS

 **ORCID:** 0000-0002-5014-2993

 **E-mail:** apdemirov@misys.ru

Дмитрий Сергеевич Белов – к.т.н., ст. науч. сотрудник кафедры функциональных наносистем и высокотемпературных материалов, НИТУ МИСИС

 **ORCID:** 0000-0002-7053-5540

 **E-mail:** dm.blv@yandex.ru

Виктор Сергеевич Сергеевич – к.т.н., инженер кафедры функциональных наносистем и высокотемпературных материалов, НИТУ МИСИС

 **ORCID:** 0000-0002-7053-5540

 **E-mail:** v.s.sergevnin@gmail.com

Александр Павлович Демиров – ассистент кафедры функциональных наносистем и высокотемпературных материалов, НИТУ МИСИС

 **ORCID:** 0000-0002-5014-2993

 **E-mail:** apdemirov@misys.ru

Contribution of the Authors



Вклад авторов

A. V. Chernogor – formation of the basic concept, statement of the purpose and objectives of the study, preparation of the text, formulation of conclusions, conducting experiments on deposition of coatings.

I. V. Blinkov – scientific guidance, text editing and conclusions.

D. S. Belov – analysis of research results, preparation of illustrative material, conducting experiments to study the physicochemical properties of coatings.

V. S. Sergevnin – carrying out tribological studies of samples with coatings.

A. P. Demirov – conducting research on the structure and composition of coatings, providing resources.

А. В. Черногор – формирование основной концепции, постановка цели и задачи исследования, подготовка текста, формулирование выводов, проведение экспериментов по осаждению покрытий.

И. В. Блинков – научное руководство, редактирование текста и выводов.

Д. С. Белов – анализ результатов исследований, подготовка иллюстративного материала, проведение экспериментов по изучению физико-механических свойств покрытий.

В. С. Сергеевич – проведение трибологических исследований образцов с покрытиями.

А. П. Демиров – проведение исследований структуры и состава покрытий, обеспечение ресурсами.

Received 27.07.2022

Revised 07.11.2022

Accepted 10.11.2022

Статья поступила 27.07.2022 г.

Доработана 07.11.2022 г.

Принята к публикации 10.11.2022 г.